Time-lapse full-waveform inversion for cases with seawater or near-surface velocity changes

Xin Fu and Kris Innanen

ABSTRACT

Time-lapse (4D) seismic full-waveform inversion (FWI) can provide high-resolution imaging of reservoir changes caused by the production of hydrocarbon (e.g., enhanced oil recovery) and the unground storage of CO_2. However, successful seismic monitoring depends on good repeatability between baseline and monitor surveys. However, the capacity of time-lapse FWI technology on solving the non-repeatability issue of seawater or near-surface velocity changes during baseline and monitor seismic surveys has not been demonstrated. In this paper, we investigate the capability of the parallel strategy, the double-difference strategy, the sequential strategy, and the common-model strategy in the non-repeatability issue of seawater or near-surface velocity changes using synthetic time-lapse marine streamer data, time-lapse OBN (ocean-bottom node) data, and time-lapse surface land data. The investigation shows that when using marine streamer data, both the double-difference strategy and the common-model strategy can adapt to relatively small seawater changes, and only the common-model strategy can adapt to relatively big seawater changes; when using OBN data, the parallel strategy, the double-difference strategy, and the common-model strategy all can adapt to relatively small seawater changes, and the best result is given by the double-difference strategy, but none of them can adapt to relatively big seawater changes; when using surface land data, the common-model strategy can adapt to the random near-surface changes best.

INTRODUCTION

Applying time-lapse (4D) seismic methods for reservoir monitoring and characterization has developed for a long time since the mid-late 1980s (Greaves and Fulp, 1987; Lumley, 2001; Landrø, 2001; Calvert, 2005; Hicks et al., 2016; Jack, 2017; Cho and Jun, 2021), which can be employed to monitor reservoir changes caused by the production of hydrocarbon (e.g., enhanced oil recovery) and the unground storage of CO_2. Especially, due to the increasing demand for technologies to control greenhouse gas emissions, storing CO_2 in the subsurface has been being developing by many researchers, and 4D seismic methods are used to monitor the CO_2 storages accordingly (Egorov et al., 2017; Cho and Jun, 2021; Ajo-Franklin et al., 2013; Macquet et al., 2019). However, successful seismic monitoring depends on the repeatability between baseline and monitor surveys that can be affected by variations in weather conditions, source and receiver positions, environmental noises, source wavelets, seawater or near-surface properties, etc.

The impact of the variations can be alleviated by good acquisition plans and/or proper processing, e.g., repeatable acquisition geometries and data processing procedures. To obtain good repeatable data to monitor the reservoir changes, the permanent OBC (ocean-bottom-cable) installations are set at Foinhaven and Valhall fields (Calvert, 2005; Yang et al., 2016). And at the Aneth oil field in Utah, the receivers are cemented in the monitor well to acquire time-lapse VSP (vertical seismic profile) data (Cheng et al., 2010). In

the CO2CRC Otway field experiment, Shulakova et al. (2015) improve the repeatability of the land seismic data by burying the receivers which can lower the noises caused by poor weather conditions, non-repeatable receiver positions, near-surface changes, and non-repeatable survey environments. During the data processing, a cross-equalization method is often applied to enhance the repeatability between baseline and monitor data (Rickett and Lumley, 2001). Fu et al. (2020) propose a double-wavelet method to eliminate the source wavelet non-repeatability which can also be reduced by designing a matching filter (Fu and Innanen, 2022c). In past years, time-lapse seismic surveys based on a fiber-optic distributed acoustic sensing (DAS) system becomes increasingly popular, since the down-hole DAS array can be permanently installed, has lower monitoring cost, and is of finer spatial sampling (Zwartjes et al., 2018; Byerley et al., 2018; Wilson et al., 2021).

As a powerful tool for 4D seismic data inversion to monitor subsurface reservoir changes and/or CO_2 storages, full waveform inversion (FWI) (Lailly et al., 1983; Tarantola, 1984; Virieux and Operto, 2009) has the ability of high-resolution imaging of physical properties for subsurface media, and it can solve the problem of non-repeatable receiver/source positions in time-lapse seismic surveys (Zhou and Lumley, 2021b). In the past decade, many time-lapse FWI methods have been developed. The most conventional time-lapse FWI strategy is the parallel strategy (Lumley et al., 2003; Plessix et al., 2010), but its result is prone to be affected by the convergence difference (Yang et al., 2015) and non-repeatable receiver/source positions (Zhou and Lumley, 2021b; Fu and Innanen, 2022a) between baseline and monitor inversion. Routh et al. (2012) present the sequential strategy, using the inverted baseline model as a starting model for monitor inversion, which can help to save computational cost and has been justified in a field VSP data case (Egorov et al., 2017). However, this strategy often generates strong artifacts since it enhances the convergence difference between twice FWIes (Yang et al., 2015; Zhou and Lumley, 2021b). But a local-updating sequential strategy can efficiently reduce the artifacts and perform well in both synthetic and field time-lapse data (Raknes and Arntsen, 2014; Asnaashari et al., 2015). Also, the local-updating method can be incorporated with the double-difference strategy, which will be introduced later, to improve the time-lapse results (Zhang and Huang, 2013; Li et al., 2021), alleviate the impact of taking an acoustic approximation to elastic subsurface rocks (Willemsen et al., 2016), or implement Bayesian/Markov Chain Monte Carlo formulation of time-lapse FWI (Fu and Innanen, 2022b). And the local-solver-based local-updating method can significantly decrease the computational cost of time-lapse FWI (Willemsen, 2017; Huang et al., 2018; Kotsi et al., 2020). Of course, the local-updating method needs prior location information about reservoir change, which may be difficult to be obtained in some cases of non-repeatable time-lapse surveys, such as the ones in this study.

The double-difference strategy, directly minimizing residuals between synthetic difference data (synthetic monitor data minus synthetic baseline data) and observed difference data (observed monitor data minus observed baseline data), applied in 4D FWI first by Zheng et al. (2011), has been adopted by several researchers (Zhang and Huang, 2013; Raknes and Arntsen, 2014; Yang et al., 2015; Willemsen et al., 2016; Fu and Innanen, 2021) including a real data case in Yang et al. (2016). It can focus on reservoir changes and reduce artifacts outside the reservoir, hence, its result is not sensitive to the convergence degree of the inverted baseline model. Nevertheless, the double-difference strategy requires

well repeated time-lapse surveys. Fu et al. (2020) introduce a double-wavelet method to handle the case of non-repeatable baseline and monitor source wavelets. But the double-difference strategy is still vulnerable to the non-repeatability of receiver/source positions. The common-model strategy, presented by Hicks et al. (2016), can also decay the artifacts caused by the divergence difference between baseline and monitor inversions (Fu and Innanen, 2022a). Its philosophy is employing the same relatively well-converged starting model for baseline and monitor FWIes to guide them into the same local minimum, and it has been applied in field cases in Hicks et al. (2016) and Bortoni et al. (2021). Moreover, Maharramov et al. (2016) present a joint method in which baseline and monitor models are simultaneously inverted; Zhou and Lumley (2021a) propose a central-difference strategy containing two sequential strategies; and Fu and Innanen (2022a) build a stepsize-sharing strategy by sharing stepsizes between baseline and monitor inversions, which can eliminate the artifacts linked to the convergence difference and is suitable when the starting model is biased. However, in all the methods mentioned above, none has demonstrated that it can solve the non-repeatability issue of seawater or near-surface velocity changes during baseline and monitor seismic surveys.

In this paper, we will investigate some present time-lapse FWI strategies under the cases of non-repeatable seawater or near-surface velocities during time-lapse seismic surveys, and the purpose of our study is to find a solution for these non-repeatability issues. First, we will review the FWI technology and some present time-lapse strategies. Then we will use numerical examples to compare various strategies and conclude our observations. The synthetic seismic data used to perform these investigations will include marine streamer data, OBN (ocean-bottom node) data, and surface land data.

TIME-LAPSE FWI METHODS

Full-waveform inversion

A standard FWI (Lailly et al., 1983; Tarantola, 1984; Virieux and Operto, 2009) is minimizing the L2 norm misfit function:

$$E(\mathbf{m}) = \frac{1}{2}||\mathbf{d}_{obs} - \mathbf{F}(\mathbf{m})||_2^2, \tag{1}$$

where $\mathbf{d}_{obs}$ is the observed data or recorded wavefields, $\mathbf{F}(\cdot)$ is a forward modeling operator based on the wave equation, and $\mathbf{m}$ is the updating model (e.g., P-wave velocity).

By a linearized optimization (e,g, steepest descent method, conjugate gradient method, etc.), the model is updated iteratively as:

$$\mathbf{m}^k = \mathbf{m}^{k-1} + \delta\mathbf{m}^k, \tag{2}$$

where k is the iteration number, and

$$\delta\mathbf{m}^k = \mu^k \mathbf{g}(\mathbf{m}^{k-1}, \mathbf{d}_{res}^{k-1}), \tag{3}$$

where

$$\mathbf{d}_{res}^{k-1} = \mathbf{d}_{obs} - \mathbf{F}(\mathbf{m}^{k-1}), \tag{4}$$

in which $\mathbf{g}(\mathbf{m}^{k-1}, \mathbf{d}_{res}^{k-1})$ is the updating direction of model in iteration k, which depends on the updated model $\mathbf{m}^{k-1}$ and data residual $\mathbf{d}_{res}^{k-1}$ in iteration $k-1$. For different optimizations, it has different calculations, for instance, in the steepest descent method, $\mathbf{g}$ represents the gradient of the misfit function (equation 1) with respect to $\mathbf{m}$, which is the zero-lag cross-correlation between forward wavefileds and backward wavefields of data residuals. For the first iteration, a starting model $\mathbf{m}^0$ have to be prepared, which can be obtained by velocity analysis or tomography.

In this study, we will typically use a time-domian constant-density acoustic finite-difference method as the forward modeling operator, the steepest descent method as the optimization, and the gradient is preconditioned with the diagonal approximation of the Hessian matrix (Shin et al., 2001).

Tested time-lapse inversion strategies

In the introduction section, we have introduced the parallel strategy, the sequential strategy, the double-difference strategy, the common-model strategy, the central-difference strategy, the stepsize-sharing strategy, and the joint method. Exhaustively testing all the methods is too resource-intensive. Hence, in this study, we only test the three typical strategies (the parallel strategy, the sequential strategy, and the double-difference strategy), and the common-model strategy that has been applied in a case with minor seawater velocity changes in Hicks et al. (2016).

Parallel strategy

As the most conventional time-lapse inversion strategy, the parallel strategy, , with workflow illustrated in Figure 1a, includes two independent FWI processes. One is for baseline model inversion, and inputs are the baseline data and a starting model. Another one is for monitor model inversion, and inputs are the monitor data and the same starting model as that in the baseline model inversion. Then the inverted time-lapse model is the inverted monitor model subtract the inverted baseline model. Since FWI is highly non-linear and is easy to be stuck in different minima, the two FWI processes mentioned above often have different convergences and yield many artifacts on the final time-lapse inversion.

Sequential strategy

The sequential strategy, with workflow illustrated in Figure 1b, has the same baseline model inversion as the PRS, using baseline data and a starting model to obtain the baseline model. But the second time inversion, monitor model inversion, is different, in which the inverted baseline model is sequentially employed as the starting model for the monitor model inversion. Then the inverted monitor model minus the inverted baseline model is the time-lapse model.

Double-difference strategy

The double-difference strategy, with workflow illustrated in Figure 1c, also contains twice FWI processes. This first one is still the baseline model inversion, the same as that in the parallel strategy or sequential strategy. In the second monitor model inversion, the starting model is the inverted baseline model, same as the sequential strategy, but the input monitor data are not the observed monitor data which are altered to the composited data:

$$\mathbf{d}_{DD} = \mathbf{F}(\mathbf{m}_{bas}) + (\mathbf{d}_{mon} - \mathbf{d}_{bas}), \tag{5}$$

where $\mathbf{F}(\mathbf{m}_{bas})$ is the synthetic data of inverted baseline model $\mathbf{m}_{bas}$, $(\mathbf{d}_{mon} - \mathbf{d}_{bas})$ is the difference data (observed monitor data $\mathbf{d}_{mon}$ subtract observed baseline data $\mathbf{d}_{bas}$). Accordingly, the misfit function for monitor model inversion becomes:

$$\mathbf{E}_{DD}(\mathbf{m}_{mon}) = \frac{1}{2}||\mathbf{d}_{DD} - \mathbf{F}(\mathbf{m}_{mon})||_2^2, \tag{6}$$

where $\mathbf{F}(\mathbf{m}_{mon})$ is the synthetic data of inverted monitor model $\mathbf{m}_{mon}$.

Common-model strategy

The common-model strategy, with workflow illustrated in Figure 1d, can be seen as an upgraded version of the strategy. Essentially, it contains twice parallel strategies. Firstly, the baseline and monitor model inversions are performed independently with the same starting model. Then a new starting model is taken from the average of baseline and monitor models, with which the baseline and monitor model inversions are performed independently again, still using the original data sets. And the final time-lapse change is obtained from the difference of baseline and monitor models in the second-time parallel strategy.

Note that in the original version of the common-model strategy in Hicks et al. (2016), the first-time parallel strategy only uses low-frequency seismic components, and only high-frequency seismic components are employed in the second-time parallel strategy. It may cause a low-frequency component lack in the final inverted time-lapse change. Hence, we use all-frequency seismic components for every single FWI process to enhance the original version.

NUMERICAL EXAMPLES

Marine streamer seismic data tests

To simulate marine streamer time-lapse seismic data, modified acoustic Marmousi models (P-wave velocities) are used to build a time-lapse model in Figures 2a-c, which includes a baseline model (Figure 2a) and a monitor model (Figure 2b). Time-lapse changes, equal monitor model minus baseline model, are plotted in Figure 2c. And the reservoir velocity changes are located at the top of the bottom anticline of the model, which is constantly $150m/s$. And a $300\ m$ seawater layer with a constant P-wave velocity of $1500\ m/s$ is on the top, which is an approximation to the real case. Model parameters for the baseline model and monitor model are identical. The model spacing is $10m$, and the model size is

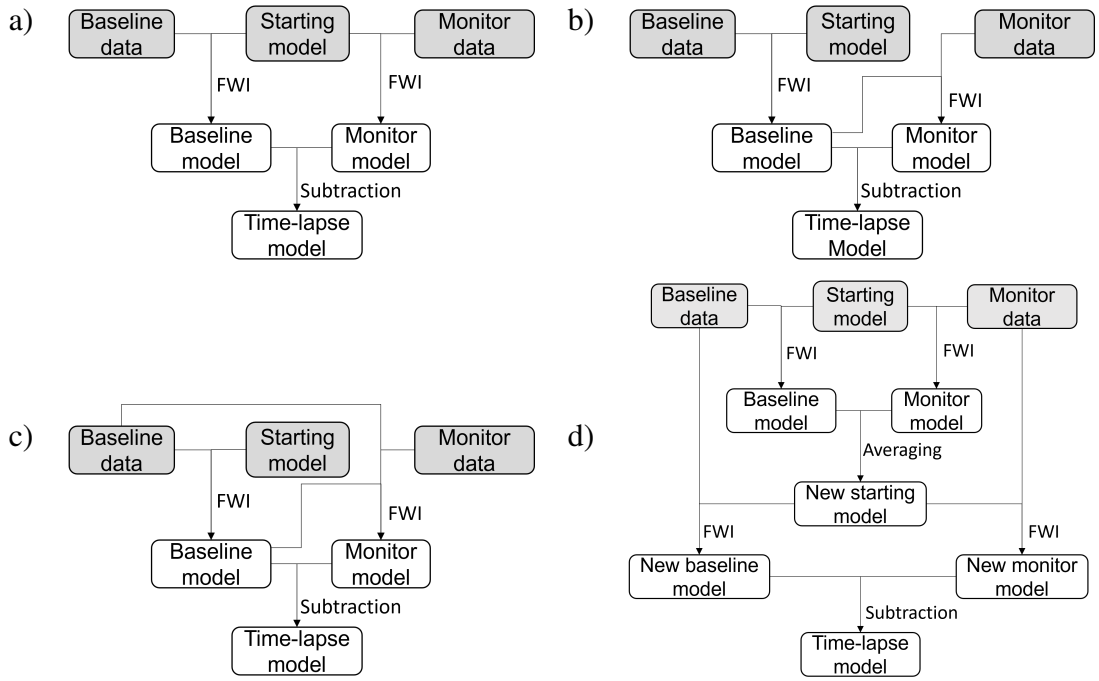

FIG. 1. Workflows of (a) the parallel strategy, (b) the sequential strategy, (c) the double-difference strategy, and (d) the common-model strategy.

188-by-327. Ten sources are evenly spread on the top, and 327 receivers are also located on each cell grid at the top. A $15Hz$ Ricker wavelet is adopted as the source wavelet. And baseline and monitor surveys are perfectly repeated, so we can make our study concentrate on non-repeatable seawater velocities.

The case with no seawater velocity changes

In Figure 3a, a model smoothed from the true baseline model (Figure 2a) is plotted, which is employed as the starting model for all strategies. The curve of data misfit versus iteration number and the first inverted baseline model are plotted in Figures 3b and c, respectively. The data misfit is completely converged, and the inverted baseline model is well recovered and can nicely match the true model. Better convergences of baseline and monitor inversions can provide better time-lapse change estimation. In Figures 4a-d, inverted time-lapse changes of various strategies from marine streamer seismic data for the marine time-lapse model with no seawater velocity changes (Figure 2a-b) are plotted. In Figure 4c, artifacts are full in the result of the sequential strategy, and the time-lapse changes cannot be recognized. The result of parallel strategy (Figure 4a) also contains many artifacts, especially in the high-velocity anomaly area which has lower convergence. The results of the double-difference strategy (Figure 4b) and the common-model strategy (Figure 4d) both can focus on the time-lapse change and have weak artifacts. The former values are closer to the true reservoir changes, but the latter has fewer artifacts.

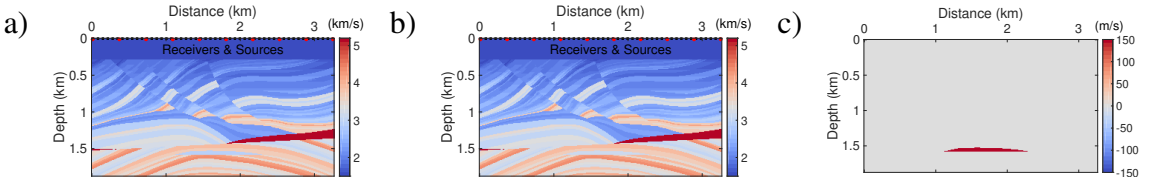

FIG. 2. The marine time-lapse model: (a) baseline model and (b) monitor model. (c) The time-lapse change ($150m/s$). There is no seawater velocity change. Sources and receivers, located on the top of the model, are denoted with red asterisks and black dot lines, respectively.

Cases with seawater velocity changes

The case in Figure 2a-c is that with no seawater velocity changes. But in a more realistic case, seawater velocity changes often happen since the seawater velocity (v_{water}) varies with water temperature(T), salinity(S), and depth(D), which can be different at different times. Especially, water temperature is a key point for the changes according to Medwin (1975) equation:

$$v_{water} = 1449.2 + 4.6T - 0.055T^2 + 0.00029T^3 + (1.34 - 0.01T)(S - 35) + 0.016D. \quad (7)$$

Hence we add some seawater velocity changes to the monitor model (Figure 2). The corresponding time-lapse changes after adding the velocity changes are plotted in Figure 5a-c respectively, in which the maximum velocity changes are, respectively, $10\ m/s$, $20\ m/s$, and $50\ m/s$ at depth zero. Their corresponding surface temperature changes are about $2\ ^\circ C$, $4\ ^\circ C$, and $11\ ^\circ C$, respectively, if we assume the salinity and depth of seawater are invariant. And the velocity changes linearly decrease with depth increase, the minimum velocity changes at depth $300\ m$ are only 4% of the maximum ones.

In Figures 6a-d, 7a-d, and 8a-d, inverted time-lapse changes of various strategies for the marine time-lapse models with maximum seawater velocity changes of $10\ m/s$, $20\ m/s$, and $50\ m/s$ are plotted, respectively. The sequential strategy still does not work. From the results in Figures 6-7, we observe even small seawater changes can cause strong artifacts in the result of the parallel strategy; and in the results of the double-difference strategy and the common-model strategy, which contain much fewer artifacts, the time-lapse changes can be clearly distinguished, and the seawater changes can also be reflected in them. And in Figure 8, the time-lapse change can only be recognized in the result of the common-model strategy, but the result also comes with some artifacts. All in all, artifacts become more serious with the increase of seawater velocity change, the double-difference strategy can adapt to relatively small seawater changes, and the common-model strategy is suitable for relatively strong seawater changes.

Ocean-bottom node seismic data tests

In this subsection, the time-lapse models utilized in the above subsection (Figure 2-8) are also used. The only difference is in the acquisition geometry, and the one employed in this subsection to generate OBN seismic data is illustrated in Figure 9. Ten sources are evenly spread on the top, and 327 receivers are located on each cell grid at the seabed.The curve of data misfit versus iteration number and the first inverted baseline model are plotted in Figures 10b and c, respectively. The data misfit is completely converged, and the inverted

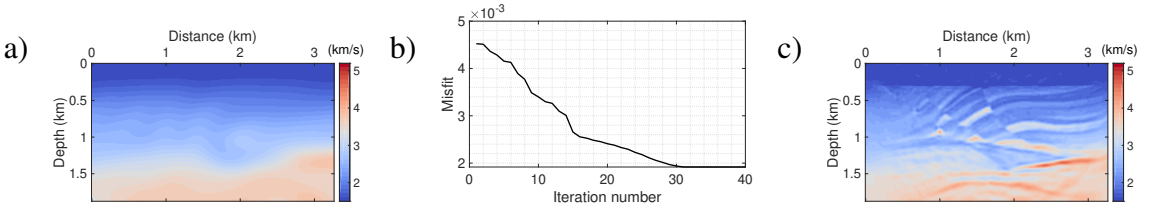

FIG. 3. The first baseline inversion for surface marine seismic data. (a) The smooth starting model. (b) The curve of data misfit versus iteration number during the baseline inversion. (c) The final inverted baseline model. Data misfit has completely converged.

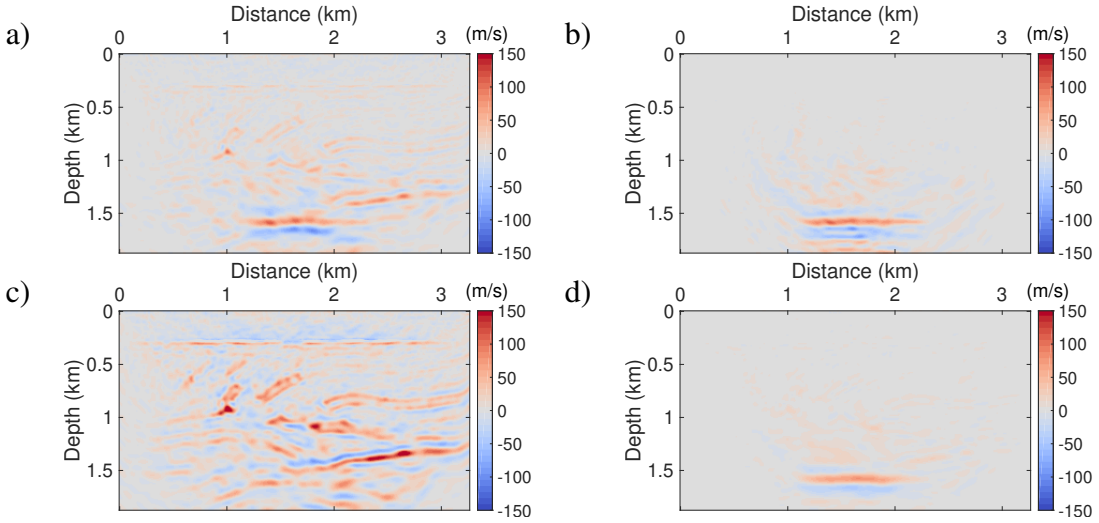

FIG. 4. The inverted time-lapse changes of various strategies from surface marine seismic data for the marine time-lapse model with no seawater velocity change. (a) the parallel strategy, (b) the double-difference strategy, (c) the sequential strategy , and (d) the common-model strategy.

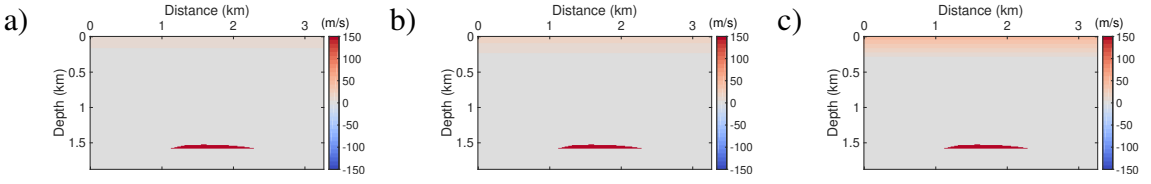

FIG. 5. The time-lapse changes of three marine time-lapse models with different seawater velocity changes. The time-lapse models are the same as those in Figure 2a-b, except for (a) $10m/s$, (b) $20m/s$, and (c) $50m/s$ constant seawater velocity changes, respectively, added to the monitor models.

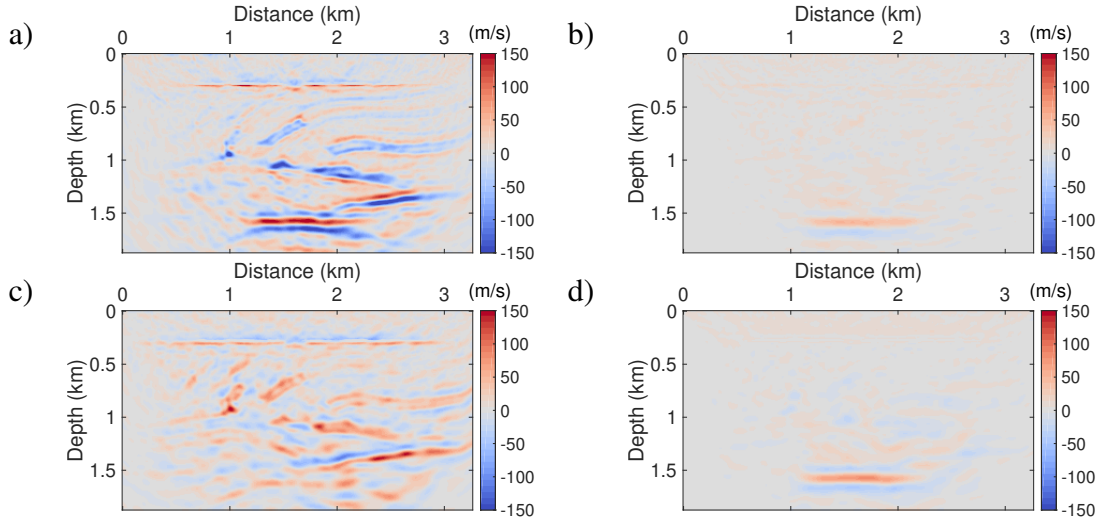

FIG. 6. The inverted time-lapse changes of various strategies from surface marine seismic data for the marine time-lapse model with a $10m/s$ seawater velocity change. (a) the parallel strategy, (b) the double-difference strategy, (c) the sequential strategy , and (d) the common-model strategy.

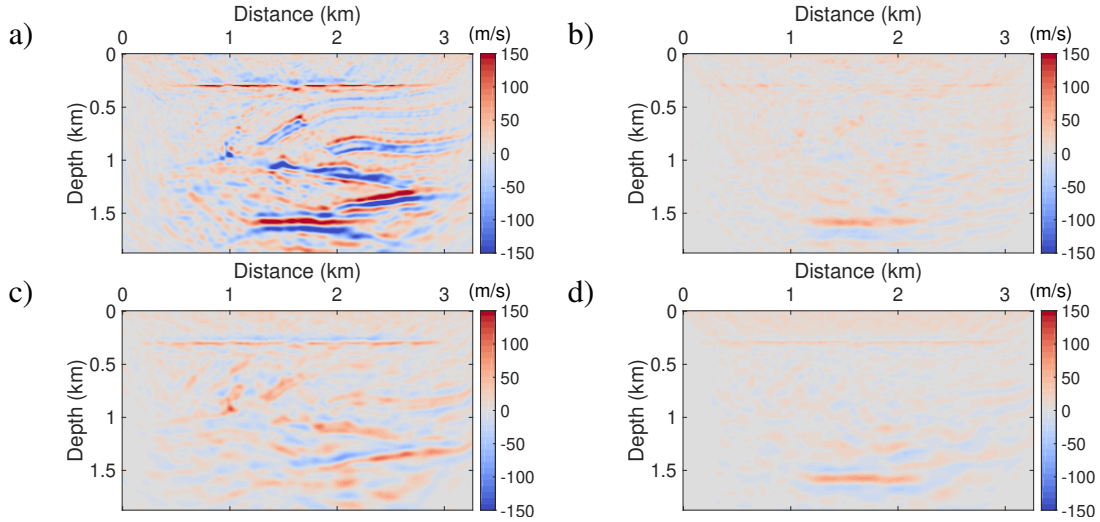

FIG. 7. The inverted time-lapse changes of various strategies from surface marine seismic data for the marine time-lapse model with a $20m/s$ seawater velocity change. (a) the parallel strategy, (b) the double-difference strategy, (c) the sequential strategy , and (d) the common-model strategy.

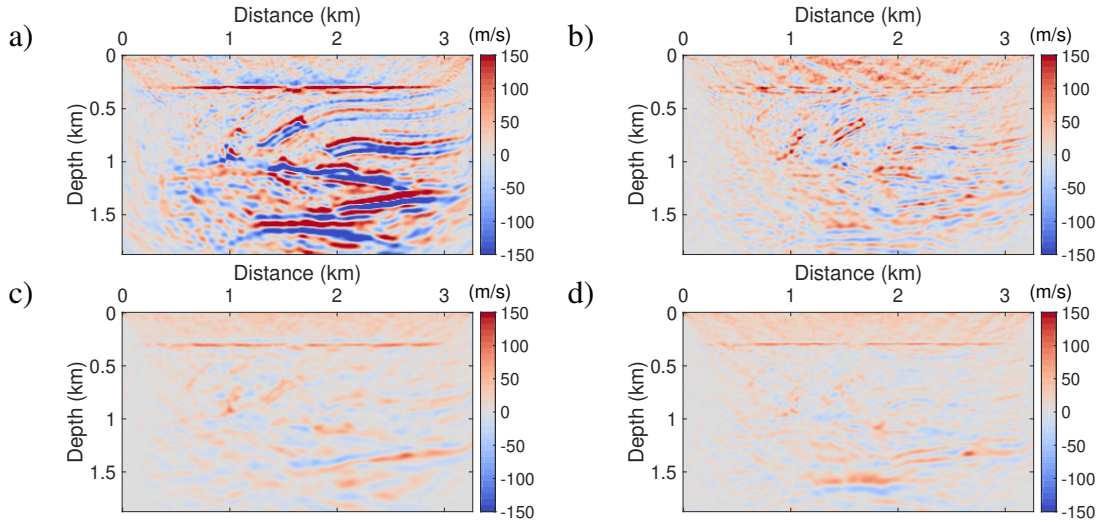

FIG. 8. The inverted time-lapse changes of various strategies from surface marine seismic data for the marine time-lapse model with a $50m/s$ seawater velocity change. (a) the parallel strategy, (b) the double-difference strategy, (c) the sequential strategy , and (d) the common-model strategy.

baseline model is well recovered.

The case with no seawater velocity changes

The inverted time-lapse changes of various strategies from OBN seismic data for the marine time-lapse model with no seawater velocity changes are plotted in Figure 11a-d. We observe, except for the sequential strategy, the performance of other strategies is similar, all can generate good time-lapse estimates with few artifacts outside the reservoir area. Comparison between Figures 4a and 11a illustrates that the parallel strategy performs better in OBN data than the marine streamer data, and has much fewer artifacts caused by the convergence difference between baseline and monitor inversions.

Cases with seawater velocity changes

The inverted time-lapse changes of various strategies from OBN seismic data for the marine time-lapse models with $10\ m/s$, $20\ m/s$, and $50\ m/s$ maximum seawater velocity changes are, respectively, plotted in Figure 12, 13, and 14. In Figures 12 and13, we observe except for the sequential strategy, all other strategies have successfully estimated time-lapse changes including reservoir changes and seawater velocity changes. But in Figure 8, the time-lapse change can only be recognized from the result of the double-difference strategy. In total, artifacts become more serious with the increase of seawater velocity changes, both the parallel strategy and the common-model strategy can adapt to relatively small seawater changes, and only the double-difference strategy is suitable for relatively strong seawater changes.

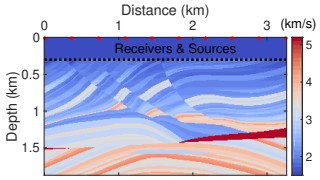

FIG. 9. The baseline model and acquisition geometry of a marine time-lapse model in which baseline model, monitor model, and source locations (red asterisks) are identical to those in Figure 2a-b. But all receivers (the black dot line) are located on the seabed at a depth of $300m$ to obtain OBN seismic data.

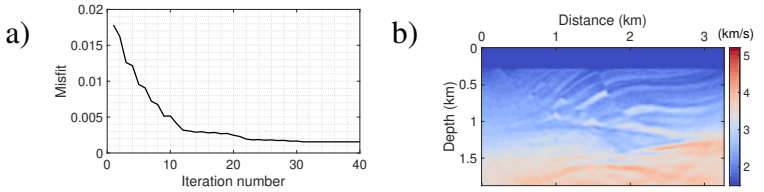

FIG. 10. The baseline inversion result from OBN data. (a) The plot of data misfit versus iteration number during the baseline inversion. (b) The final inverted baseline model. Data misfit has completely converged.

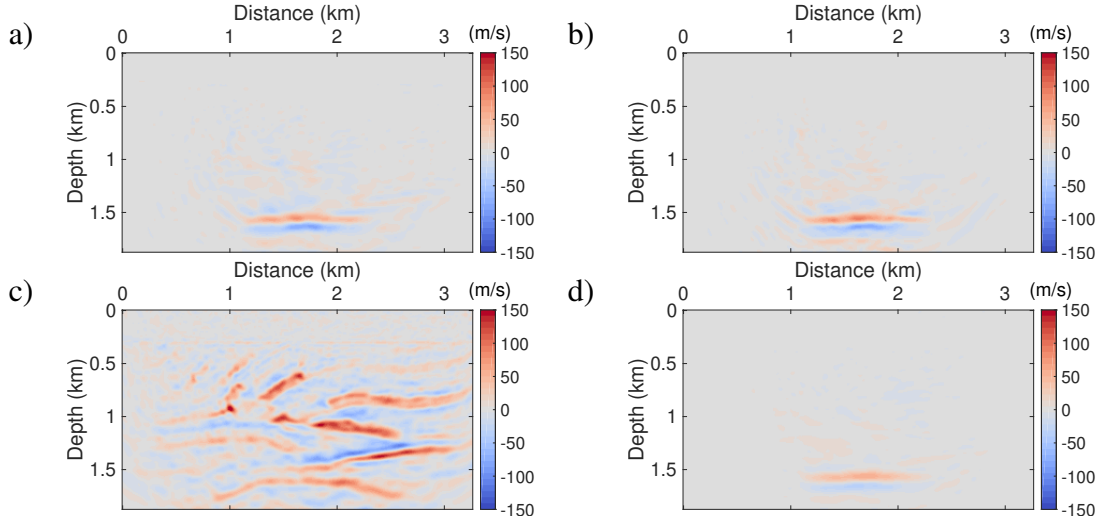

FIG. 11. The inverted time-lapse changes of various strategies from OBN seismic data for the marine time-lapse model with no seawater velocity change. (a) the parallel strategy, (b) the double-difference strategy, (c) the sequential strategy , and (d) the common-model strategy.

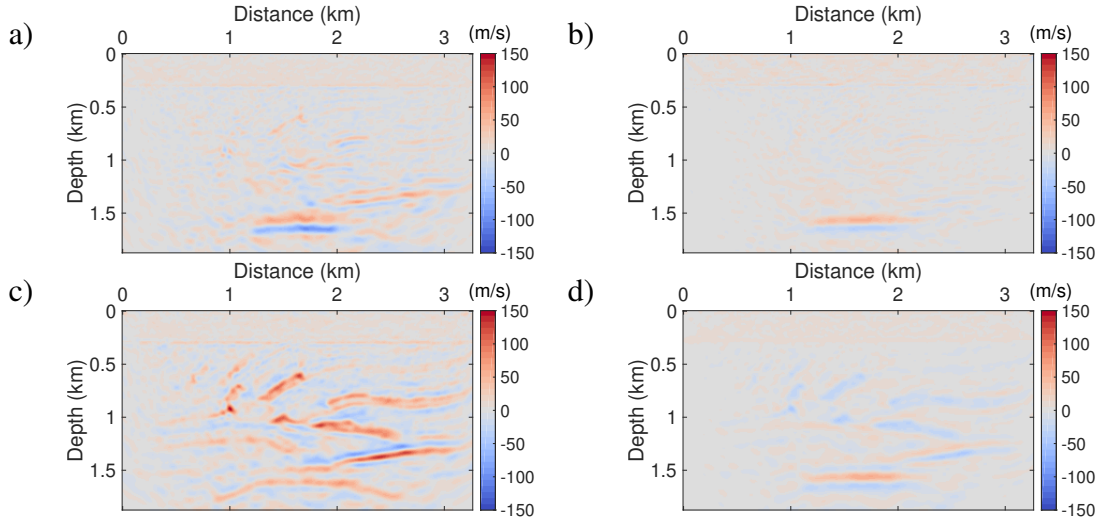

FIG. 12. The inverted time-lapse changes of various strategies from OBN seismic data for the marine time-lapse model with a $10m/s$ seawater velocity change. (a) the parallel strategy, (b) the double-difference strategy, (c) the sequential strategy, and (d) the common-model strategy.

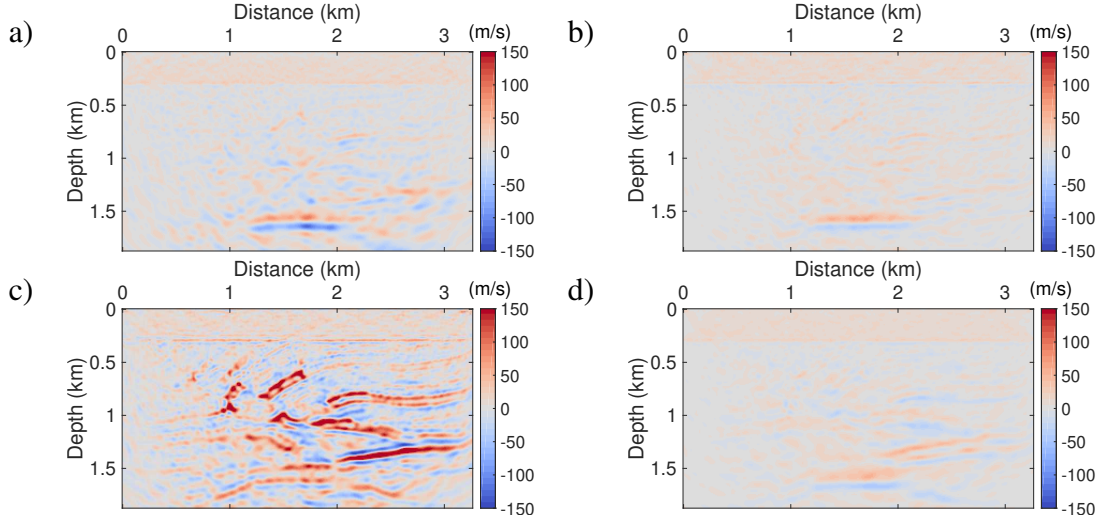

FIG. 13. The inverted time-lapse changes of various strategies from OBN seismic data for the marine time-lapse model with a $20m/s$ seawater velocity change. (a) the parallel strategy, (b) the double-difference strategy, (c) the sequential strategy, and (d) the common-model strategy.

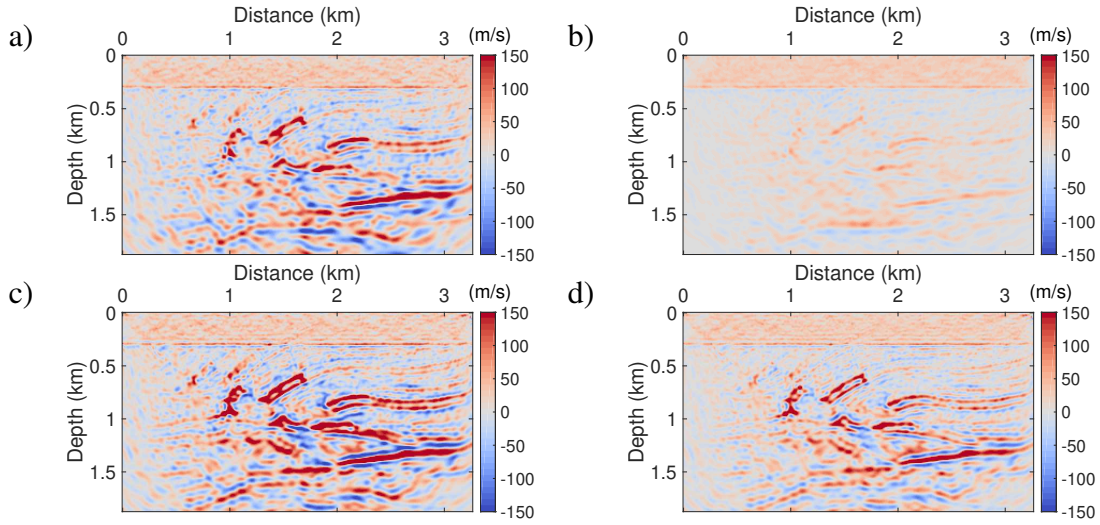

FIG. 14. The inverted time-lapse changes of various strategies from OBN seismic data for the marine time-lapse model with a $50m/s$ seawater velocity change. (a) the parallel strategy, (b) the double-difference strategy, (c) the sequential strategy, and (d) the common-model strategy.

Surface land seismic data tests

In this subsection, surface land time-lapse seismic data are applied to test the strategies. The model used is a land acoustic time-lapse model including a baseline model and a monitor model plotted in Figure 15a and b. The model is free of near-surface changes, and the corresponding time-lapse changes are plotted in Figure 15c. The model and acquisition parameters in Figure 15 are the same as that in Figure 2, except for the water layer being removed in Figure 15 when compared with Figure 2. Again, the starting model, the curve of data misfit versus iteration number, and the first inverted baseline model are plotted in Figures 16a-c, respectively. The data misfit is completely converged, and the inverted baseline model is well recovered.

The case with no near-surface velocity changes

The inverted time-lapse changes of various strategies from surface land seismic data for the land time-lapse model with no near-surface velocity changes (Figure 15) are plotted in Figure 17a-d. We observe results of the double-difference strategy and the common-model strategy are very similar, which contain few artifacts outside the reservoir area, artifacts in the result of the parallel strategy are much heavier, and the sequential strategy still does not work.

The case with near-surface velocity changes

To test the cases with near-surface velocity changes, random near-surface velocity changes plotted in Figure 18b are added to the near-surface part of the monitor model (Figure 15b), and the corresponding time-lapse changes of the new time-lapse land model are plotted in Figure 18a. And the inverted time-lapse changes of various strategies for the land time-lapse model with random near-surface velocity changes are plotted in Figure

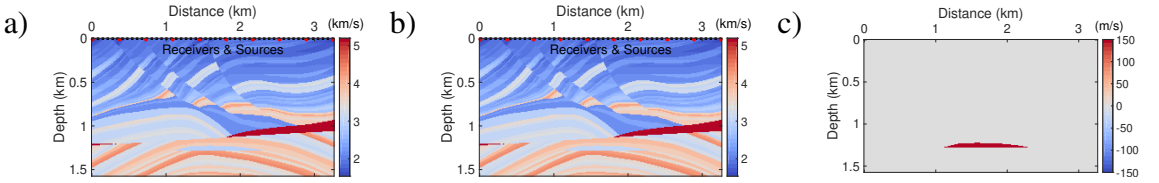

FIG. 15. The land time-lapse model: (a) baseline model and (b) monitor model. (c) The time-lapse change ($150m/s$). There is no near-surface velocity change. Sources and receivers, located on the top of the model, are denoted with red asterisks and black dot lines, respectively.

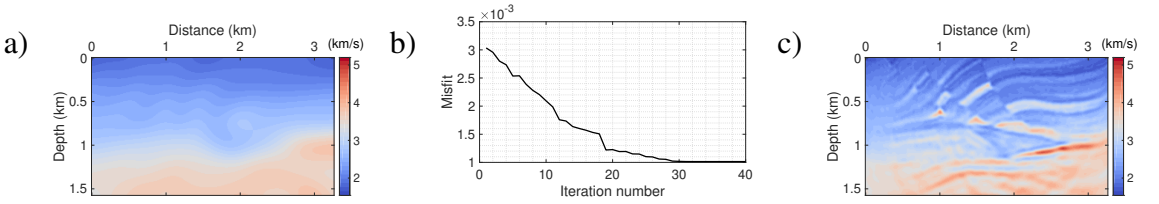

FIG. 16. Baseline inversion results for the land time-lapse model. (a) The smooth starting model. (b) The plot of data misfit versus iteration number during the baseline inversion. (c) The final inverted baseline model. Data misfit has completely converged.

19a-d. We observe that the best result is given by the common-model strategy, where the reservoir changes are easy to be recognized but also with some artifacts; in the results of the parallel strategy and the double-difference strategy, some artifacts are comparable to the inverted reservoir changes, and they are difficult to be distinguished from each other; again, the sequential strategy does not work.

DISCUSSION

In this study, we focus on the non-repeatability issue of seawater or near-surface velocity changes, in practice more non-repeatability issues could be encountered, such as the issues of non-repeatable noises, non-repeatable receiver/source positions, non-repeatable source wavelets, and biased starting model. For more researches involving these issues, readers can refer to Zhou and Lumley (2021b), Fu and Innanen (2022c), and Fu and Innanen (2022a).

For OBN time-lapse data, the double-difference strategy performs better than others. However, it is too sensitive to non-repeatabilities of receiver/source positions and source wavelets (Fu et al., 2020; Zhou and Lumley, 2021b). Hence in more general cases, the parallel strategy or the common-model strategy is more adaptive. And more superior methods should be developed to enhance the capability of time-lapse FWI technology, especially in cases of big seawater velocity changes.

CONCLUSION

We have investigated the capability of the parallel strategy, the double-difference strategy, the sequential strategy, and the common-model strategy in the non-repeatability issue of seawater or near-surface velocity changes using synthetic marine streamer data, OBN data, and surface land data. The investigation shows that when using marine streamer data, both the double-difference strategy and the common-model strategy can adapt to relatively small seawater changes, and only the common-model strategy can adapt to relatively big

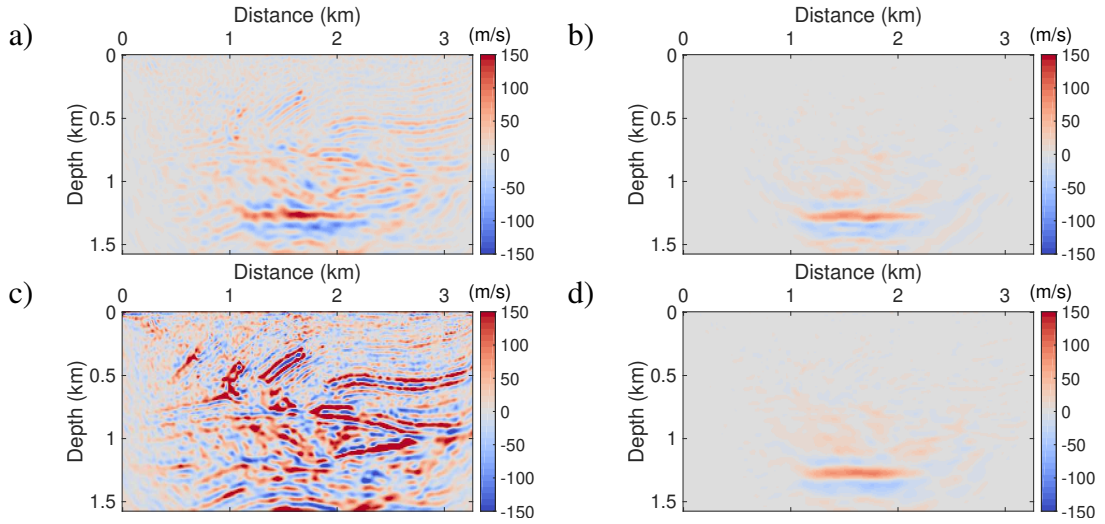

FIG. 17. The inverted time-lapse changes of various strategies from surface land seismic data for the land time-lapse model with no near-surface velocity change. (a) the parallel strategy, (b) the double-difference strategy, (c) the sequential strategy, and (d) the common-model strategy.

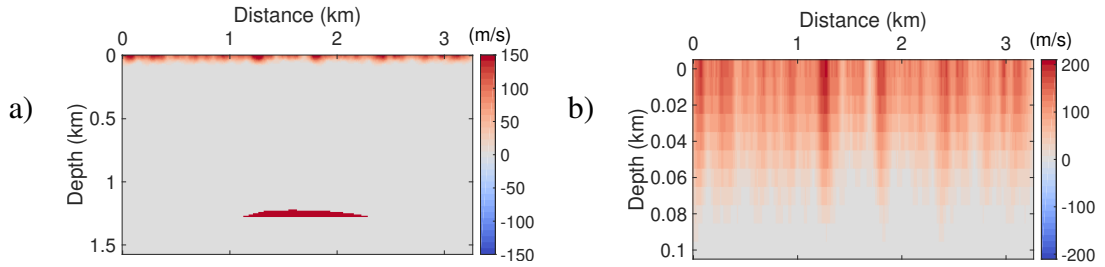

FIG. 18. (a) The time-lapse changes of land time-lapse models with random near-surface velocity changes. The time-lapse model is the same as that in Figure 15a-b, except for the random near-surface velocity changes added to the monitor models. (b) Zoomed in near-surface velocity changes in (a).

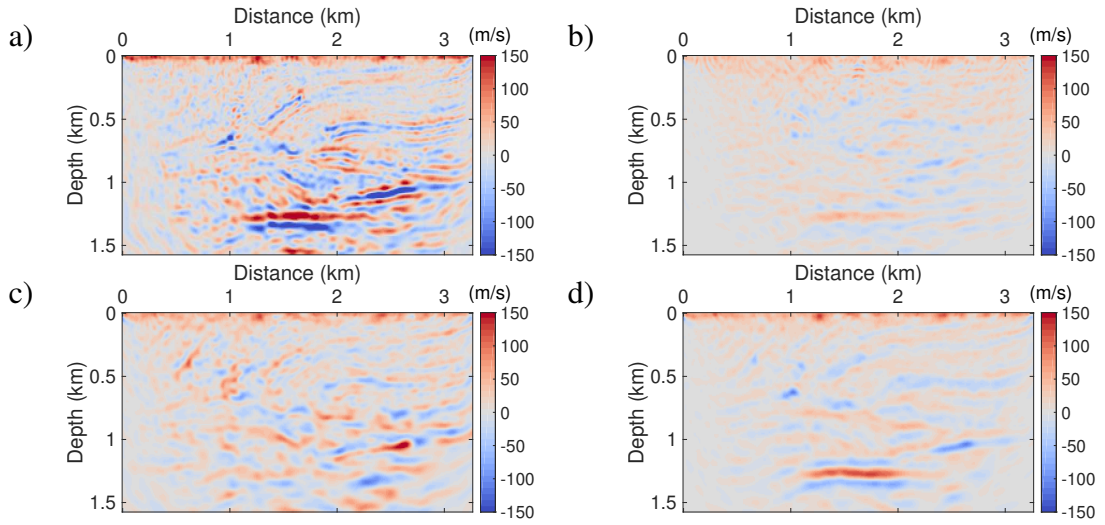

FIG. 19. The inverted time-lapse changes of various strategies from near-surface land seismic data for the land time-lapse model with random near-surface velocity changes. (a) The parallel strategy, (b) the double-difference strategy, (c) the sequential strategy, and (d) the common-model. strategy.

seawater changes; when using OBN data, the parallel strategy, the double-difference strategy, and the common-model strategy all can adapt to relatively small seawater changes, and the best result is given by the double-difference strategy, but none of them can adapt to relatively big seawater changes; when using surface land data, the common-model strategy can adapt to the random near-surface changes best.

ACKNOWLEDGEMENTS

We thank the sponsors of CREWES for continued support. This work was funded by CREWES industrial sponsors, NSERC (Natural Science and Engineering Research Council of Canada) through the grants CRDPJ 461179-13 and CRDPJ 543578-19. Partial funding also came from the Canada First Research Excellence Fund.

REFERENCES

Ajo-Franklin, J., Peterson, J., Doetsch, J., and Daley, T., 2013, High-resolution characterization of a co2 plume using crosswell seismic tomography: Cranfield, ms, usa: International Journal of Greenhouse Gas Control, **18**, 497–509.

Asnaashari, A., Brossier, R., Garambois, S., Audebert, F., Thore, P., and Virieux, J., 2015, Time-lapse seismic imaging using regularized full-waveform inversion with a prior model: which strategy?: Geophysical prospecting, **63**, No. 1, 78–98.

Bortoni, S., Barragan, S., Azevedo, G., Cypriano, L., Ferreira, A., Moreira, W., dos Reis, P., and Filho, W., 2021, Learnings from an fwi imaging study using 3d and 4d data over a postsalt field in campos basin, *in* First International Meeting for Applied Geoscience & Energy, Society of Exploration Geophysicists, 587–591.

Byerley, G., Monk, D., Aaron, P., and Yates, M., 2018, Time-lapse seismic monitoring of individual hydraulic frac stages using a downhole das array: The Leading Edge, **37**, No. 11, 802–810.

Calvert, R., 2005, Insights and methods for 4D reservoir monitoring and characterization: Society of Exploration Geophysicists and European Association of ....

Cheng, A., Huang, L., and Rutledge, J., 2010, Time-lapse vsp data processing for monitoring co 2 injection: The Leading Edge, **29**, No. 2, 196–199.

Cho, Y., and Jun, H., 2021, Estimation and uncertainty analysis of the co2 storage volume in the sleipner field via 4d reversible-jump markov-chain monte carlo: Journal of Petroleum Science and Engineering, **200**, 108,333.

Egorov, A., Pevzner, R., Bóna, A., Glubokovskikh, S., Puzyrev, V., Tertyshnikov, K., and Gurevich, B., 2017, Time-lapse full waveform inversion of vertical seismic profile data: Workflow and application to the co2crc otway project: Geophysical Research Letters, **44**, No. 14, 7211–7218.

Fu, X., and Innanen, K. A., 2021, An mcmc-based approach to time-lapse full-waveform inversion, *in* First International Meeting for Applied Geoscience & Energy, Society of Exploration Geophysicists, 3484–3489.

Fu, X., and Innanen, K. A., 2022a, Stepsize sharing in time-lapse full-waveform inversion, *in* Second International Meeting for Applied Geoscience & Energy, Society of Exploration Geophysicists, 473–477.

Fu, X., and Innanen, K. A., 2022b, A time-domain, multi-source bayesian/markov chain monte carlo formulation of time-lapse seismic waveform inversion: Geophysics, **87**, No. 4, 1–110.

Fu, X., and Innanen, K. A., 2022c, Time-lapse seismic imaging using shot gathers with non-repeatable source wavelets: Geophysics, **88**, No. 1, 1–108.

Fu, X., Romahn, S., and Innanen, K., 2020, Double-wavelet double-difference time-lapse waveform inversion, *in* SEG Technical Program Expanded Abstracts 2020, Society of Exploration Geophysicists, 3764–3767.

Greaves, R. J., and Fulp, T. J., 1987, Three-dimensional seismic monitoring of an enhanced oil recovery process: Geophysics, **52**, No. 9, 1175–1187.

Hicks, E., Hoeber, H., Houbiers, M., Lescoffit, S. P., Ratcliffe, A., and Vinje, V., 2016, Time-lapse full-waveform inversion as a reservoir-monitoring tool—a north sea case study: The Leading Edge, **35**, No. 10, 850–858.

Huang, X., Jakobsen, M., Eikrem, K. S., and Nævdal, G., 2018, A target-oriented scheme for efficient inversion of time-lapse seismic waveform data, *in* 2018 SEG International Exposition and Annual Meeting, OnePetro.

Jack, I., 2017, 4d seismic—past, present, and future: The Leading Edge, **36**, No. 5, 386–392.

Kotsi, M., Malcolm, A., and Ely, G., 2020, Uncertainty quantification in time-lapse seismic imaging: a full-waveform approach: Geophysical Journal International, **222**, No. 2, 1245–1263.

Lailly, P., Bednar, J. et al., 1983, The seismic inverse problem as a sequence of before stack migrations: Conference on Inverse Scattering, Theory and Application, Society for Industrial and Applied Mathematics, Expanded Abstracts, 206–220.

Landrø, M., 2001, Discrimination between pressure and fluid saturation changes from time-lapse seismic data: Geophysics, **66**, No. 3, 836–844.

Li, Y., Alkhalifah, T., and Guo, Q., 2021, Target-oriented time-lapse waveform inversion using deep learning-assisted regularization: Geophysics, **86**, No. 4, R485–R495.

Lumley, D., Adams, D. C., Meadows, M., Cole, S., and Wright, R., 2003, 4d seismic data processing issues and examples, *in* SEG Technical Program Expanded Abstracts 2003, Society of Exploration Geophysicists, 1394–1397.

Lumley, D. E., 2001, Time-lapse seismic reservoir monitoring: Geophysics, **66**, No. 1, 50–53.

Macquet, M., Lawton, D. C., Saeedfar, A., and Osadetz, K. G., 2019, A feasibility study for detection thresholds of co2 at shallow depths at the cami field research station, newell county, alberta, canada: Petroleum Geoscience, **25**, No. 4, 509–518.

Maharramov, M., Biondi, B. L., and Meadows, M. A., 2016, Time-lapse inverse theory with applicationstime-lapse inverse theory: Geophysics, **81**, No. 6, R485–R501.

Medwin, H., 1975, Speed of sound in water: A simple equation for realistic parameters: The Journal of the Acoustical Society of America, **58**, No. 6, 1318–1319.

Plessix, R.-E., Michelet, S., Rynja, H., Kuehl, H., Perkins, C., de Maag, J., and Hatchell, P., 2010, Some 3d applications of full waveform inversion, *in* 72nd EAGE Conference and Exhibition-Workshops and Fieldtrips, European Association of Geoscientists & Engineers, cp–162.

Raknes, E. B., and Arntsen, B., 2014, Time-lapse full-waveform inversion of limited-offset seismic data using a local migration regularization: Geophysics, **79**, No. 3, WA117–WA128.

Rickett, J., and Lumley, D., 2001, Cross-equalization data processing for time-lapse seismic reservoir monitoring: A case study from the gulf of mexico: Geophysics, **66**, No. 4, 1015–1025.

Routh, P., Palacharla, G., Chikichev, I., and Lazaratos, S., 2012, Full wavefield inversion of time-lapse data for improved imaging and reservoir characterization, *in* SEG Technical Program Expanded Abstracts 2012, Society of Exploration Geophysicists, 1–6.

Shin, C., Jang, S., and Min, D.-J., 2001, Improved amplitude preservation for prestack depth migration by inverse scattering theory: Geophysical prospecting, **49**, No. 5, 592–606.

Shulakova, V., Pevzner, R., Dupuis, J. C., Urosevic, M., Tertyshnikov, K., Lumley, D. E., and Gurevich, B., 2015, Burying receivers for improved time-lapse seismic repeatability: Co2crc otway field experiment: Geophysical Prospecting, **63**, No. 1, 55–69.

Tarantola, A., 1984, Inversion of seismic reflection data in the acoustic approximation: Geophysics, **49**, No. 8, 1259–1266.

Virieux, J., and Operto, S., 2009, An overview of full-waveform inversion in exploration geophysics: Geophysics, **74**, No. 6, WCC1–WCC26.

Willemsen, B., Cao, J., and Roy, B., 2016, The impact of the acoustic approximation on time-lapse fwi, *in* 2016 SEG International Exposition and Annual Meeting, OnePetro.

Willemsen, L. A., 2017, Problems with a localized nature in exploration seismology: Ph.D. thesis, Massachusetts Institute of Technology.

Wilson, G. A., Willis, M. E., and Ellmauthaler, A., 2021, Evaluating 3d and 4d das vsp image quality of subsea carbon storage: The Leading Edge, **40**, No. 4, 261–266.

Yang, D., Liu, F., Morton, S., Malcolm, A., and Fehler, M., 2016, Time-lapse full-waveform inversion with ocean-bottom-cable data: Application on valhall field: Geophysics, **81**, No. 4, R225–R235.

Yang, D., Meadows, M., Inderwiesen, P., Landa, J., Malcolm, A., and Fehler, M., 2015, Double-difference waveform inversion: Feasibility and robustness study with pressure data: Geophysics, **80**, No. 6, M129–M141.

Zhang, Z., and Huang, L., 2013, Double-difference elastic-waveform inversion with prior information for time-lapse monitoring: Geophysics, **78**, No. 6, R259–R273.

Zheng, Y., Barton, P., and Singh, S., 2011, Strategies for elastic full waveform inversion of time-lapse ocean bottom cable (obc) seismic data, *in* SEG Technical Program Expanded Abstracts 2011, Society of Exploration Geophysicists, 4195–4200.

Zhou, W., and Lumley, D., 2021a, Central-difference time-lapse 4d seismic full-waveform inversion: Geophysics, **86**, No. 2, R161–R172.

Zhou, W., and Lumley, D., 2021b, Nonrepeatability effects on time-lapse 4d seismic full-waveform inversion for ocean-bottom node data: Geophysics, **86**, No. 4, R547–R561.

Zwartjes, P., Mateeva, A., Chalenski, D., Duan, Y., Kiyashchenko, D., and Lopez, J., 2018, Frequent, multi-well, stand-alone 3d das vsp for low-cost reservoir monitoring in deepwater, *in* SEG Technical Program Expanded Abstracts 2018, Society of Exploration Geophysicists, 4948–4952.